Examining origins of magnetic anomalies at the crystal scale using scanning magnetic microscopy

Church, N. S. [1], McEnroe, S. A.[1]

1. NTNU, Trondheim, Norway

ABSTRACT

Scanning magnetic microscopy (SMM) maps the magnetic field generated by petrologic thin sections or polished rock surfaces at the sub-mm scale, creating the possibility to resolve the contribution of individual grains and mineral phases to bulk magnetic signal. The instrument developed at NTNU has the capability to measure both remanence properties and, uniquely, the magnetic response in a field of known magnitude and direction. A series of case studies are presented to examine the capabilities of the microscope and to describe applications to the study of crustal magnetism. The use of well-characterized samples allows signals in magnetic scans to be attributed to grains of known composition, including the discrimination of signal associated with discrete oxides and assemblages of exsolved oxides in silicates, which can be observed to have differing directions of magnetisation. The ability of this instrument to image in fields mimicking those experienced in the crust allows the observation of the induced magnetic response, both qualitatively in the form of changes in magnetization direction, and quantitatively by varying experimental conditions. This capability gives SMM the ability to map both remanent response and generate a map of susceptibility, and provides a powerful new tool for the examination of bulk magnetic response in the Earth's crust.

INTRODUCTION

Scanning magnetic microscopy (SMM) is a developing technique that creates a spatial map of the magnetic field measured in a horizontal plane above polished rock surfaces or petrologic thin sections, analogous to an aeromagnetic survey at a sub-millimetre scale (e.g. Egli & Heller 2000; Weiss et al., 2007; Hankard et al., 2009). At such a spatial resolution, SMM can be used to identify the contribution of individual mineral grains or assemblages of fine particles to the bulk magnetic properties of natural samples. It represents a powerful new tool for the identification and characterization of the carriers of NRM and the induced response in crustal magnetism studies. Further studies may extend these capabilities to examination of the paleomagnetic directions of individual phases and grains, offering time-resolved information about the creation of bulk remanence signals.

EXPERIMENTAL SETUP & CAPABILITIES

The instrument developed at NTNU uses room-temperature magnetic tunnel junction sensors and implements the electronics package and lock-in technique described by Lima et al. (2014) with further modifications to the circuit design. Unlike aeromagnetic surveys, SMM does not directly measure the total magnetic intensity: only a single component of the field (here the vertical component, B_z) is observed. The data presented in this article are single-component maps of B_z (positive upwards). The remaining components can be calculated if desired (Lima & Weiss 2009). Magnetic tunnel junction sensors are generally less sensitive than fluxgate or proton precession magnetometers used in aeromagnetic surveys, or superconducting quantum interference devices (SQUIDs) used in SMM of extremely weak samples. However, this lack of sensitivity is partially offset by scanning very close to the sample surface. The scans presented here were acquired at a constant height of 100 μm above the sample, and greater sensitivity can be achieved by using a smaller scanning distance down to direct contact with the surface.

In addition to higher sensitivity, close scanning enhances spatial resolution of fine features. The scanning stage used in the NTNU instrument is a non-magnetic piezoelectric unit with a precision of >10 nm. The effective spatial resolution of the magnetic scan is therefore limited largely by scan height, desired scan time (the scans presented here required 4—8 hours) and the active area of the sensor, which acts to convolve the magnetic signal over its area. The high-sensitivity sensor used here has an active area of 900 μm. In future work we plan to implement a sensor that permits closer scanning with an active area of only 2 μm.

Unlike most scanning magnetic microscopes, the NTNU instrument employs active field control via Helmholtz coils rather than having the instrument situated in a shielded room. The advantage of the Helmholtz coils is that they allows for imaging in controlled fields ranging from <10 nT to 100 μT, approximately twice that found at the surface of the Earth. The magnitude and geometry of the field can be set at the start of the scanning. The ability to measure at near-zero field, or in a constant field of known direction and intensity allows the acquisition of purely remanent signals, or of combined remanent

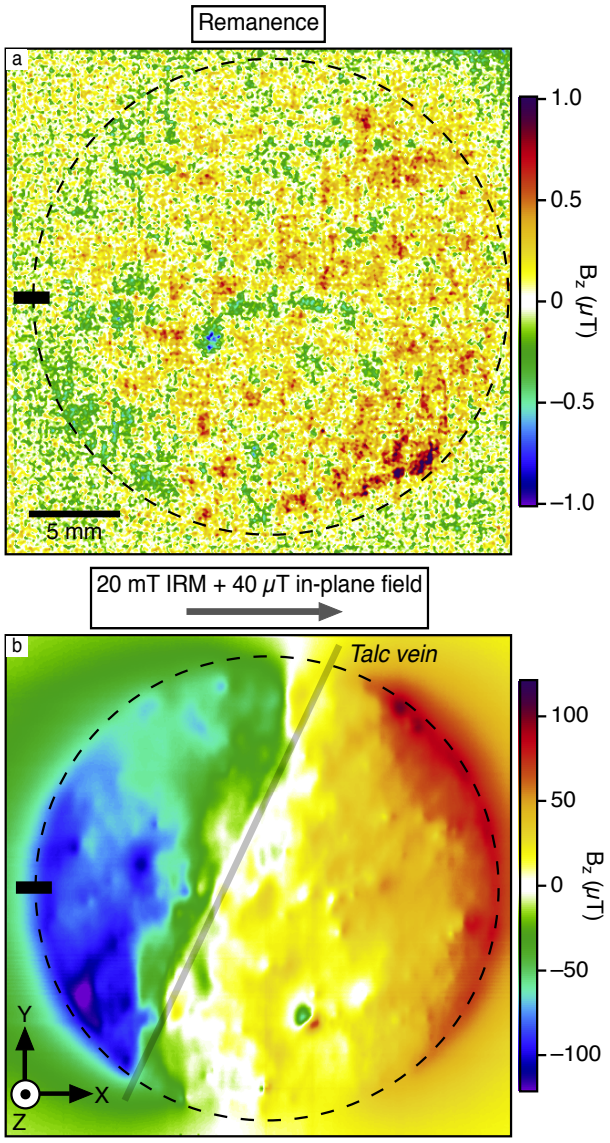

Figure 1. Dunite paleomagnetic core. The dashed line indicates edge of core; black rectangle at left of sample is strike line to indicate orientation in both scans. a) Scan of demagnetized state, at zero field. b) Scan following pulse remagnetization in +X direction and acquired in a field also in +X.

and induced signals mimicking the behavior of the sample in the Earth's crust. Subtraction of the remanent signal allows one to calculate maps of purely induced magnetization. Such an approach was described early in the SMM literature by Thomas et al. (1992), but was not pursued as the rock magnetic community prioritised greater sensitivity to weak remanence signals.

The ability to measure induced and remanent magnetization independently is one of several possible experiments that aid in interpretation of SMM data. While inversions and forward modelling of SMM data are subject to the same non-uniqueness challenges as for crustal anomalies, the use of discrete samples creates the possibility to make other measurements that serve as constraints for the proposed models. Commonly the positions of the most strongly magnetic phases can be known, either using light microscopy with thin sections or computed tomography of thicker samples, and an absolute maximum depth is known from the thickness of the sample. The total magnetization of the specimen can be measured in a moment magnetometer, and samples can be demagnetized or remagnetized in a known direction with scans acquired at each step to observe differing behavior of individual magnetic grains and phases. This process can be carried out incrementally to reveal the contribution of low- and high-coercivity phases independently. Finally, with certain experimental setups (small sensor area, thin sample, relatively high scan height) the geometry of the magnetization model can be considered two-dimensional, greatly reducing degrees of freedom of the inversion.

CASE STUDIES

Instrument performance

Figure 1 demonstrates the flexibility and sensitivity of the magnetic tunnel junction sensor. While non-cryogenic sensors cannot offer the dynamic range and low-field sensitivity of SQUIDs, they are sufficient to measure the magnetic response of rock samples containing abundant magnetic particles. The sample shown in Figure 1 is a paleomagnetic core (25 mm diameter, 22 mm height) of a serpentinized dunite from the Reinfjord ultramafic intrusion (Grant et al., 2016) in northern Norway, with the scan acquired at 100 µm height. It contains extensive alteration at the micro- and macro-scale, including a near-vertical talc vein that intersects the top surface as indicated in Figure 1b and reflects a high degree of serpentinization.

The core was previously demagnetized in alternating fields up to 200 mT (unbeknownst to the scanning microscope operator). As the sample was almost completely demagnetized (bulk magnetization of 0.250 A/m), the scan in Figure 1a is an illustration of the limits of the scanning magnetic microscope's capabilities with extremely weak samples. The region well outside the sample boundaries represents the noise floor of the sensor, which is 0.25 µT RMS, consistent with visual estimations. Despite the sample's demagnetized state, there are still measurable signal that creates visible structure to the field, particularly the positive signals in the right half of the sample. In the absence of good characterization of the minerals at the surface of the core it is difficult to attribute this signal to a magnetic phase.

As discussed above, one of the tools available in SMM to constrain interpretations of magnetic sources is the ability to remagnetize the sample in a known direction. Figure 1b is a scan of the same sample previously demagnetized after giving it an isothermal remanent magnetization (IRM) in a field of 20 mT in the +X direction. The scan was acquired in a field of 40 µT in the same direction to prevent relaxation of low-coercivity particles, and is presented in the same orientation as that of Figure 1a. The sample has clearly acquired a magnetization in plane in the direction of the IRM and applied field. The signal is 2 orders of magnitude higher than that of the demagnetized sample and 3 orders of magnitude higher than the noise floor. A limited number of magnetic features are clear at the surface, such as the

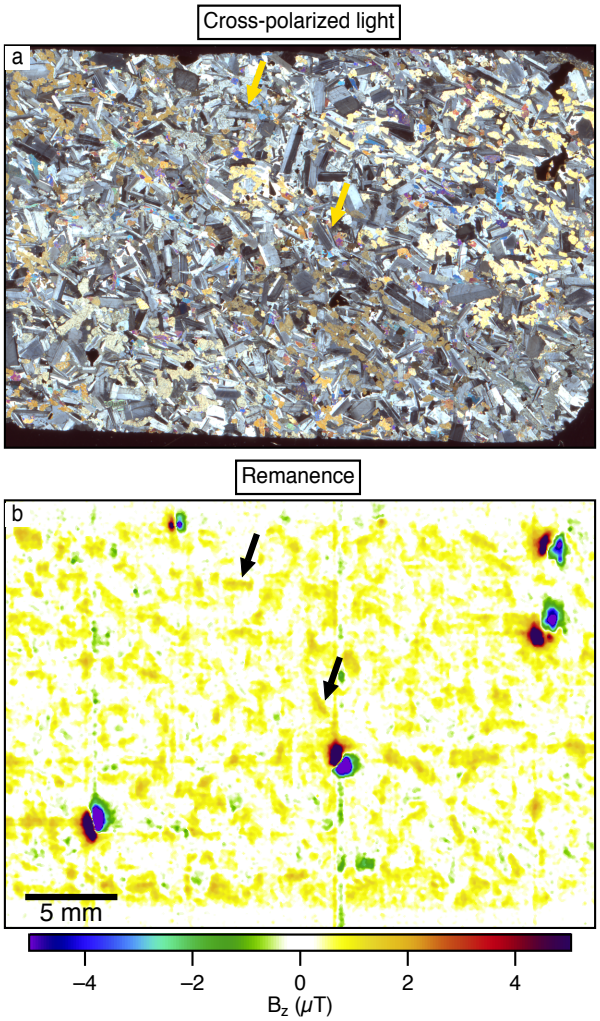

Figure 2. Thin section of gabbro-norite from the Bushveld intrusion. Magnetic phases include discrete oxides and plagioclase crystals bearing abundant exsolved magnetite. a) Cross-polarised light image. b) SMM scan. Strongest signals are associated with discrete oxides, but arrows indicate lath-shaped magnetic signals that can be attributed to plagioclase crystals visible in Figure 2a.

dipole structure in the lower right quadrant. This feature is not obviously aligned with the overall magnetization of the sample, although interpretation of the direction of magnetization may be complicated by the overall magnetization of the sample as a whole. A vein of talc visible in the sample is noted on Figure 1b; as it is evidence of high levels of serpentization this phase was expected to be associated with enhanced magnetic signal due to high levels of magnetite formation. The magnetic scan does not obviously have stronger magnetization, but the trace of the vein appears as a linear feature in the scan.

Discriminating contributions from individual mineral phases

One of the motivations for acquiring spatially-resolved maps of magnetization using techniques such as SMM is the ability to distinguish magnetic signals associated with different phases in a complex mineral system. Samples containing both discrete

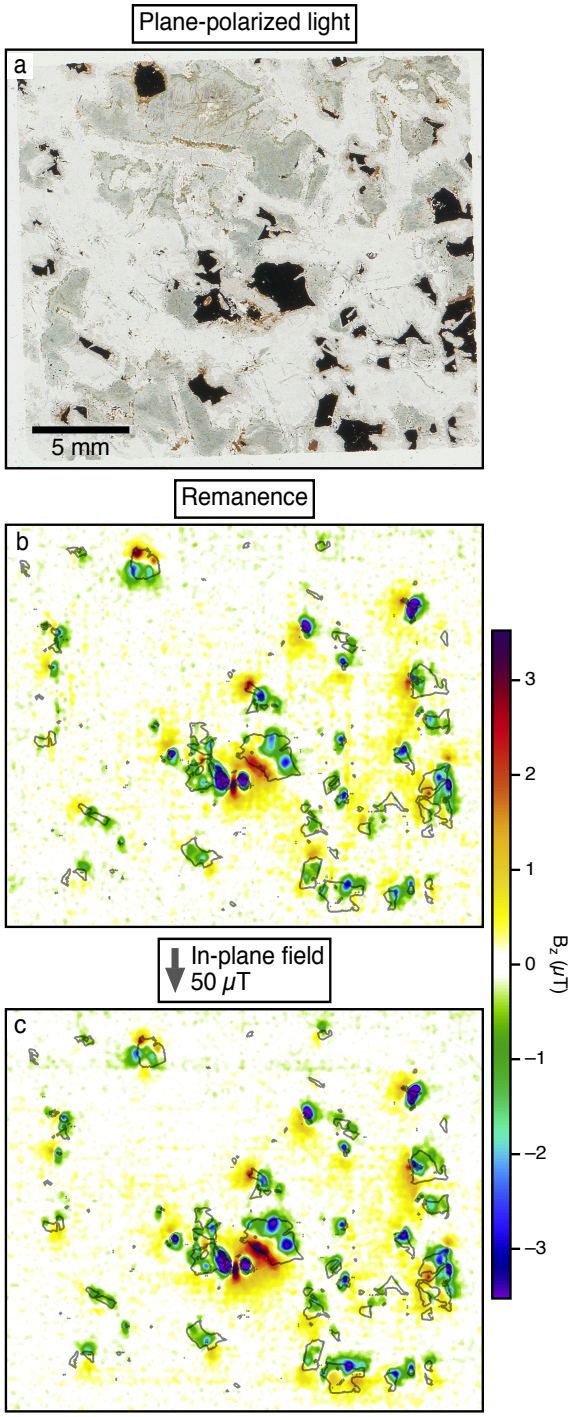

Figure 3. Thin section of meta-gabbro. a) Plane-polarised light image. b) Scan in zero field. Outlines of oxide (magnetite and ilmenite composite grains) overlaid for comparison. c) Scan with 50 µT field applied in plane of sample, in -Y direction.

magnetic oxides and elongated magnetic grains exsolved from silicates are such a system where the carriers are not only expected to have very different magnetic contributions in terms of intensity, but also will behave differently at remanence or in the Earth's ambient field. The gabbro-norites of the Main Zone of the Bushveld intrusion (South Africa) contain both discrete oxides

and abundant exsolution in both pyroxene and plagioclase, which have been attributed as the source of exceptionally stable remanence carriers (Hattingh, 1986). Sample BS1 is a thin section from the Stoffberg locality in the eastern lobe of the intrusion (Cawthorn et al,, 2016), and contains oxy-exsolved magnetite, plagioclase with abundant magnetite needles, and predominantly clean pyroxene lacking any oxide exsolution. The cross-polarised light image in Figure 2a illustrates the size of the plagioclase laths (1—3 mm in length, up to 1 mm wide) and the magnetite grains are opaque and the darkest features in the image.

The synthesis of the mineralogical data from the thin section allows the distinct magnetic remanence signals of the discrete oxides and magnetite-bearing plagioclase to be distinguished. The discrete magnetite grains are the source of the strongest signals and do not show a consistent direction of magnetization, although on aggregate have a -X trend. The magnetization is largely in the plane of the thin section (see, for example, Figure 1 of Weiss et al. 2007 for models of in-plane magnetization), which may represent a primary direction or alternatively may reflect the effect of shape anisotropy of these thin, laterally extensive and relatively easily remagnetized particles. By contrast, the signal not associated with discrete oxides is largely vertical (+Z). In several regions the shape of the magnetic signal mimics the shape of the plagioclase laths (2 such points indicated by arrows in Figures 2a and 2b), and probably derive from the abundant magnetite within them. The magnetic history of this thin section and those that follow is not well-constrained and the measured signal may reflect the use of electromagnets during the polishing process.

Comparing remanence and in-field measurements

Figure 3 presents the results of a series of scans of 1551-3B, an eclogite facies meta-gabbro from Norway (McEnroe et al., in review). The transmitted light image (Figure 3a) illustrates the location of the opaques, which are predominantly magnetite and ilmenite with exsolved hematite lamellae. The magnetite and ilmenite commonly are present as composite grains. The two lower figures are magnetic scans of the thin section, at the same spatial scale and with the outlines of the opaques for reference. The scan acquired at remanence (Figure 3b) shows no consistent direction of magnetization. Similar to the data presented in Figure 2b, the magnetization appears to be largely in the plane of the sample, which again may be a function of the shape anisotropy of particles in thin section. The magnetic fields are strongest at the edges of the grains.

Figure 3c is a scan acquired in a field of 50 µT oriented in the plane of the sample and pointing in the -Y direction (toward the bottom of the image). The color scale of both magnetic scans are the same, so the increase in intensity in many of the particles in the in-field data set represents an increase in total magnetization due to the additional induced magnetization. This effect is most apparent in the large particle in the centre of the scan, but can also be observed in others, such as those near the right side. Furthermore, the magnetization direction of a number of particles

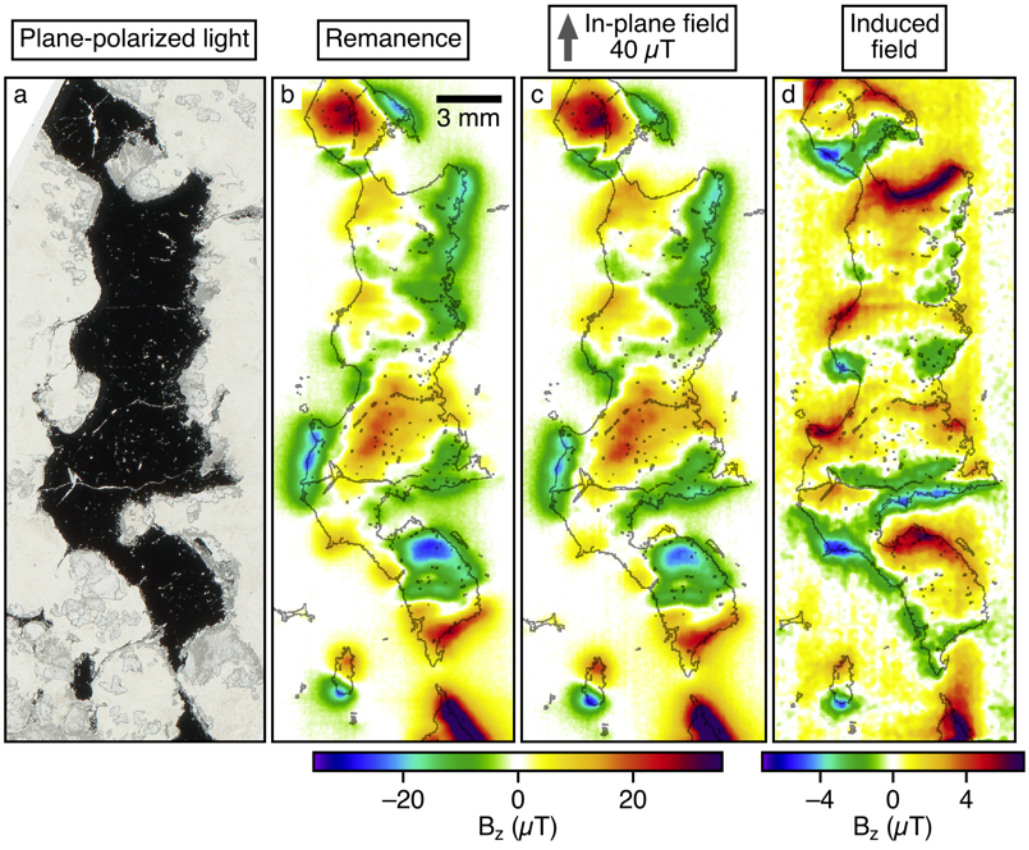

Figure 4. Thin section of a metamorphosed serpentinite containing magnesite and large magnetite. a) Plane-polarised light image. b) Zero-field scan, with outline of magnetite grains. c) Scan acquired with 40 µT in-plane field in +Y direction. d) Difference of scans in 4b and 4c, representing induced component generated by +Y field (Pastore et al., 2017).

appears to have been deflected toward that of the applied field. In the remanence scan, the large equidimensional particle near the top of the thin section appears to be magnetized in the plane of the sample and pointing toward the top of the scan. The applied field is antiparallel to this direction, and in the in-field measurement, the signal associated with this particle is both weaker and more complex than a simple dipole, suggesting that the magnetization of at least some part of the grain has rotated in response. In the in-field scan, several of the grains near the bottom also develop the distinctive positive-below, negative-above pairing that indicates magnetization in the plane of the sample and pointing downwards, i.e., in the direction of the applied field.

Figure 4 presents a similar experiment designed to maximise the response to the applied field. The sample is a metamorphosed serpentinite from southern Norway, which is composed of magnesite, serpentine, and cm-scale crystals of magnetite (Figure 4a). As the magnetite is large and does not contain secondary phases or other microstructure, it is predicted to exhibit multi-domain behavior and be highly responsive to applied fields.

The zero-field scan shown in Figure 4b is complex and challenging to interpret. The large particle that covers much the centre of the scan appears to have a net magnetization that is sometimes near-vertical and sometimes in the plane of the sample, such as near the bottom of this particle. In several places the strongest signal is concentrated at the edge of grains and there is a strong enhancement associated with the tapered grain that extends off the bottom of the scan. Some regions, such as the discrete elongated grain near the bottom left of the scan, have a net magnetization that approximates a dipole, in this case with the magnetization in the plane of the sample and pointing to the top of the scan.

Applying a field in the plane of the sample and oriented in the +Y direction (toward the top of the scan) yields a data set that is qualitatively similar to the zero-field scan, with slight variations in intensity (Figure 4c). The strength of this implementation of the scanning magnetic microscope is the ability to calculate the contribution of the induced magnetization by the subtraction of the in-field and zero-field maps by

$$B_{in-field} = B_{rem} + B_{induced}$$

$$B_{induced} = B_{in-field} - B_{rem}$$

where the remanent component (B_{rem}) is independently measured by scanning in zero field. The field generated (Figure 4d) by the induced magnetization is consistent with the applied field direction: as the field is oriented toward the top of the scan, there are regions of positive magnetic flux near the top edges of the particles and negative near the bottom. This feature is most prominent on horizontal edges (perpendicular to the applied field) and visible both at the edges of magnetite grains as well as along cracks within them. The unique ability of this instrument to make such a measurement creates the possibility to calculate an inversion for the induced response using the constraint of unidirectional magnetization, or equivalently, model for a map of susceptibility. This processing is an area of ongoing research.

REFERENCES

Cawthorn, R. G., K. L. Lundgaard, C. Tegner, and J. R. Wilson (2016), Lateral variations in plagioclase compositions, Main Zone, Bushveld Complex, South Africa: Evidence for slow mixing of magmas in basinal structures, Mineralogical Magazine, 80(2), 213–225, doi:10.1180/minmag.2015.079.7.12.

Egli, R., and F. Heller (2000), High-resolution imaging using a high-Tc superconducting quantum interference device (SQUID) magnetometer, J Geophys Res, 105(B11), 25709–25727, doi:10.1029/2000JB900192.

Grant, T. B., R. B. Larsen, L. Anker-Rasch, K. R. Grannes, M. Iljina, S. A. McEnroe, E. Nikolaisen, M. Schanche, and E. Øen (2016), Anatomy of a deep crustal volcanic conduit system; The Reinfjord Ultramafic Complex, Seiland Igneous Province, Northern Norway, Lithos, 252-253(C), 200–215, doi:10.1016/j.lithos.2016.02.020.

Hankard, F., J. Gattacceca, C. Fermon, M. Pannetier-Lecoeur, B. Langlais, Y. Quesnel, P. Rochette, and S. A. McEnroe (2009), Magnetic field microscopy of rock samples using a giant magnetoresistance-based scanning magnetometer, Geochem Geophy Geosy, 10(10), Q10Y06, doi:10.1029/2009GC002750.

Hattingh, P. J. (1986), The Paleomagnetizm of the Main Zone of the Eastern Bushveld Complex, Tectonophysics, 124(3-4), 271–295, doi:10.1016/0040-1951(86)90205-2.

Lima, E. A., and B. P. Weiss (2009), Obtaining vector magnetic field maps from single-component measurements of geological samples, J Geophys Res, 114(B6), B06102, doi:10.1029/2008JB006006.

Lima, E. A., A. C. Bruno, H. R. Carvalho, and B. P. Weiss (2014), Scanning magnetic tunnel junction microscope for high-resolution imaging of remanent magnetization fields, Meas. Sci. Technol., 25(10), 105401, doi:10.1088/0957-0233/25/10/105401.

Pastore, Z., N. S. Church, S. A. McEnroe (2017), Modelling of high resolution magnetic microscopy data: An application to a serpentine carbonate magnetite sample from Modum, Norway: International Conference on Rock Magnetism 2017, pp. 32.

Thomas, I. M., T. C. Moyer, and J. P. Wikswo Jr. (1992), High resolution magnetic susceptibility imaging of geological thin sections: Pilot study of a pyroclastic sample from the Bishop Tuff, California, U.S.A, Geophys Res Lett, 19(21), 2139–2142, doi:10.1029/92GL02322.

Weiss, B. P., E. A. Lima, L. E. Fong, and F. J. Baudenbacher (2007), Paleomagnetic analysis using SQUID microscopy, J Geophys Res, 112(B9), B09105, doi:10.1029/2007JB004940.